The thermodynamic specificity of cryptands principally resides in the dissociation rate constant, the most stable cryptate of a particular metal ion generally having the smallest value of the dissociation rate constant.[7,8,11] Such an easy generalization is complicated by the fact that there are also considerable differences in the formation rate constants. The trends in acid-catalyzed dissociation have also been discussed extensively,[9,11,18] but again, no broad generalizations are yet apparent. The present results offer general explanations for the kinetic results in terms of the conformations of the free ligands. An additional, important factor is the effect of metal ion on ligand conformation both in cryptates[51] and in the transition state. When structural evidence is available, unusual thermodynamic[6] and kinetic[11] results are often explained in terms of specific conformational effects. The specific influence of metal ions on conformational equilibria and energetics in undoubtedly one reason for the many exceptions to whatever broad thermodynamic and kinetic generalizations have been made about cryptates. This problem will be investigated in future studies.[52]

Conclusions

[111] is a relatively rigid molecule in which the lowest energy state is clearly endo-endo.

[222] is a flexible molecule characterized by facile exo-endo interconversion. Four conformations of similar strain energy exist, two endo-endo, an endo-exo, and an exo-exo. A number of conclusions can be made about cryptate formation based on the geometries of these various conformations:

(1) Cryptate complexes are endo-endo because this conformation brings the oxygens closest to the metal ion center.

A number of conclusions can be made about cryptate formation based on the geometries of these various conformations: (1) Cryptate complexes are endo-endo because this conformation brings the oxygens closest to the metal ion center. A number of conclusions can be made about cryptate formation based on the geometries of these various conformations.

(2) Acid-catalyzed dissociation occurs because protonation maintains relatively open, kinetically reactive ligand conformations.

(3) Cryptate formation is relatively slow compared with an I_d mechanism in part because not all conformations of [222] are kinetically reactive.

Acknowledgment. Support for this work by the National Institutes of Health (Grant GM 24748) and the PSC/BHE City University of New York Faculty Research Award Program is gratefully acknowledged (R.P.).

Appendix. Definition of Terms Used in (3)

K_s	force constant for bond length deformation
l	bond length
l_0	equilibrium bond length
K_B	force constant for bond angle deformations
θ	bond angle
θ_0	equilibrium bond angle
K_{SB}	force constant for stretch-bend deformations
K_{NB}	coefficient for nonbonded interactions
r_{ij}	distance between atoms i and j
R_{vdw}	sum of van der Waal's radii for atoms i and j
V_1, V_2, V_3	barriers for torsional motion
ω	torsional angle
K_d	coefficient for dipole-dipole interactions
μ_A	dipole moment of bond A
μ_B	dipole moment of bond B
X	angle between the dipoles
α, β	angles between the dipole axes along R
R	line between midpoints of the bonds
ϵ	dielectric constant, taken to be 1.5

Registry No. Cryptand 111, 37095-49-1; cryptand 222, 23978-09-8.

(51) A molecular mechanics calculation on [222] and alkali metal cryptate complexes appeared while this paper was in review (Wipff, G.; Kollman, P. *Nouv. J. Chim.* **1985**, *9*, 457). An excellent account is given therein of the structural aspects of various metal cryptates and the relationship between the complexed and uncomplexed ligand. Our calculations based on crystal structure data as starting points are in substantial agreement with the same calculations in this work in showing that the lowest energy conformation among this set is an elongated endo-endo with the conformations derived from the ligand structures of the sodium cryptate and calcium cryptate being higher in energy by 3.4 and 11.1 kcal, respectively. We disagree only in finding that the optimized conformation beginning with the ligand structure found in the barium cryptate is just slightly higher in energy (0.7 kcal) than endo-endo (I). No conformation lower in relative strain energy than those presented here is reported.

(52) **Note Added in Proof**: The crystal structure of [111] has just been determined (Brügge, H.-J.; Carboo, D.; von Deuten, K.; Knöchel, A.; Kopf, J.; Dreissig, W. *J. Am. Chem. Soc.* **1986**, *108*, 107).

Gouterman's "Four-Orbital" Model and the MCD Spectra of High-Symmetry Metalloporphyrins

A. Ceulemans,* W. Oldenhof, C. Görller-Walrand, and L. G. Vanquickenborne

Contribution from the Department of Chemistry, University of Leuven, Celestijnenlaan 200F, B-3030 Heverlee, Belgium. *Received July 25, 1985*

Abstract: This paper offers a description of the magnetooptical properties of highly symmetric metalloporphyrins within the framework of the Gouterman "four-orbital" model. Expressions are derived for the Faraday parameters of the Q and B (Soret) transitions of the porphyrin system as a function of the energy and intensity parameters and of the angular momenta of the relevant excited states. A discussion of these results highlights the distinct roles of two competing mechanisms, which procure the Q band intensity. On the one hand this transition may steal intensity from the Soret band as a result of interstate interactions. On the other hand the zeroth order Q^0 state may also carry a non-zero transition dipole moment as a consequence of the tetragonal symmetry of the porphyrin skeleton. The latter feature is a typical characteristic of the Gouterman model and does not occur in the algebraic solution of the perimeter model for cyclic π-electron systems. In a final section MCD spectra are reported for meso- and exo-substituted zinc porphyrins and the corresponding cyanide and pyridine complexes. From these data Faraday parameters were extracted by using a Gaussian fitting procedure. Parameter shifts caused by a change of the axial ligand are shown to follow the theoretical predictions.

Gouterman's "four-orbital" model of the π-π^* transitions in porphyrins is firmly established as a simple unifying theory of porphyrin spectra.[1-4] It provides parametric expressions for the frequencies and intensities of the α-β (Q) and Soret (B) bands

0002-7863/86/1508-1155$01.50/0

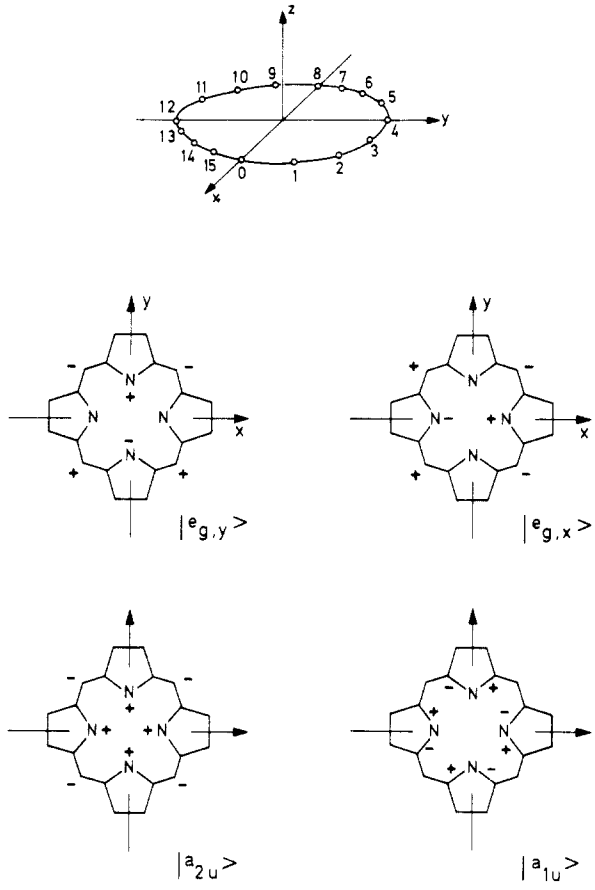

Figure 1. Top: *xyz* coordinate system and atom numbering for a 16-membered cyclic polyene. In the related porphyrin, aza substitution is at positions 0, 4, 8, and 12; ethylene bridges link positions 15–1, 3–5, 7–9, and 11–13. Center and bottom: schematic representations of the four orbitals of the Gouterman model in the usual phase convention (see ref 2); + and − signs on the inner ring indicate the phase of the p_z functions in the molecular orbitals.

of the porphyrin chromophore. Spectral shifts caused by systematic variation of ring substituents, changes of the encapsulated metal ion, axial ligation, or even dimeric formation have successfully been rationalized on these grounds.[5-8] In more recent years attention has also been devoted to the Zeeman splitting of these bands, which can be measured by the MCD (magnetic circular dichroism) technique.[9,10] Several theoretical studies of the MCD of metalloporphyrins have been published,[11-14] but apparently none of these incorporates all the premises of the original "four-orbital" model. Yet, as the present paper intends to show, rigorous application of these premises in the development of the MCD expressions leads to an improved parametric model of the MCD of metalloporphyrins.

From the outset two limitations mark the scope of this paper. First, the treatment will be confined to highly symmetric or "regular" metalloporphyrins, which exhibit tetragonal symmetry. Second, only the purely electronic zero–zero transitions, the so-called Q(0,0) and B(0,0) components, will be studied. Vibronic interactions will not be dealt with explicitly.

Table I. Standard Symmetry Behavior of the Degenerate D_{16h} Representations[a] under the Symmetry Elements[b] $C_{16,z}$ and σ_{xz}

	C_{16}[q]	σ_{xz}
$\|e_{k,c}\rangle$	$\cos(kq2\pi/16)\|e_{k,c}\rangle + \sin(kq2\pi/16)\|e_{k,s}\rangle$	$\|e_{k,c}\rangle$
$\|e_{k,s}\rangle$	$-\sin(kq2\pi/16)\|e_{k,c}\rangle + \cos(kq2\pi/16)\|e_{k,s}\rangle$	$-\|e_{k,s}\rangle$
$\|e_{k,+}\rangle$	$\exp(-ikq2\pi/16)\|e_{k,+}\rangle$	$\|e_{k,-}\rangle$
$\|e_{k,-}\rangle$	$\exp(+ikq2\pi/16)\|e_{k,-}\rangle$	$\|e_{k,+}\rangle$

[a] Parity subscripts u and g have been omitted since they do not affect the results in the table; k numbers the e representation, c and s denote real components, and + and − refer to complex components. [b] The symmetry elements are oriented in the Cartesian coordinate system of Figure 1 as indicated. The operators transform functions, rather than coordinate axes. This convention differs from Moffitt's in ref 17.

Table II. Standard Symmetry Behavior of the Components[a] of the Tetragonal e Representation under the C_{4v} Group Generators

	$C_{4,z}$	σ_{xz}
$\|e_x\rangle$	$\|e_y\rangle$	$\|e_x\rangle$
$\|e_y\rangle$	$-\|e_x\rangle$	$-\|e_y\rangle$
$\|e_+\rangle$	$-i\|e_+\rangle$	$-\|e_-\rangle$
$\|e_-\rangle$	$i\|e_-\rangle$	$-\|e_+\rangle$

[a] Parity subscripts u and g have been omitted since they do not affect the results in the table; x and y denote real components, + and − refer to complex components defined as in eq 7.

I. Outline of the "Four-Orbital" Model

The basic aspects of the "four-orbital" model have been summed up in several reviews.[2-4] In view of the delicate role of phase and space conventions in an MCD treatment, we will briefly resume explicit definitions of the relevant orbitals, states, and moments, with special attention to symmetry aspects. In a group-theoretical perspective the Gouterman model of a metalloporphyrin may be qualified as a "descent-in-symmetry" model, based on the chain $D_{16h} \rightarrow D_{4h}$. The D_{16h} parent group thereby refers to the symmetry of an idealized 16-membered cyclic polyene, matching the inner ring of the metal-containing porphyrin dianion. The D_{4h} group, which terminates the chain, corresponds to the actual molecular point group of a regular metalloporphyrin.

Coordination of an axially symmetric ligand will further reduce the molecular symmetry to C_{4v}. However, such a symmetry lowering is unimportant since it does not affect the selection rules or the band pattern of the porphyrin spectrum. Hence as far as the porphyrin chromophore is concerned, axially substituted metalloporphyrins still exhibit an effective D_{4h} symmetry and may be treated with the $D_{16h} \rightarrow D_{4h}$ model. This is not to say that axial ligands have no role to play in the Gouterman model. On the contrary, axial ligation seriously affects the energy parameters of the model and thus constitutes one of the primary variables in the experimental evaluation of the "four-orbital" model.

(a) D_{16h} Functions. Starting wave functions for the cyclic polyene are the classical π-perimeter functions of Platt and Moffitt. Refined moment calculations in this basis set have recently been performed by Michl in a general treatment of the MCD of cyclic π-electron systems.[13,15-17] A dianionc porphyrin chromophore can be approximated as a 16-membered ring carrying 18 electrons.[18] The highest occupied orbitals (HOMO) transform as e_{4u} and the lowest unoccupied ones (LUMO) as e_{5g}. Real representation components will be denoted as cos and sin, while

(1) Gouterman, M. *J. Chem. Phys.* **1959**, *30*, 1139.
(2) Gouterman, M. *J. Mol. Spectrosc.* **1961**, *6*, 138.
(3) Gouterman, M. In "The Porphyrins"; Dolphin, D., Ed.; Academic Press: New York, 1978; Vol. III, p 1.
(4) Adar, F. In "The Porphyrins"; Dolphin, D., Ed.; Academic Press: New York, 1978; Vol. III, p 167.
(5) Nappa, M.; Valentine, J. S. *J. Am. Chem. Soc.* **1978**, *100*, 5075.
(6) Wang, M.-Y. R.; Hoffman, B. M. *J. Am. Chem. Soc.* **1984**, *106*, 4235.
(7) McDermott, G. A.; Walker, F. A. *Inorg. Chim. Acta* **1984**, *91*, 95.
(8) Shelnutt, J. A. *J. Phys. Chem.* **1984**, *88*, 4988. See Also: Shelnutt, J. A.; Ortiz, V. *J. Phys. Chem.* **1985**, *89*, 4733. On p 4734 of this article the definition of r/R should read:
$$r/R = (R_2 - R_1)/(R_2 + R_1)$$
(9) Sutherland, J. C. In "The Porphyrins"; Dolphin, D., Ed.; Academic Press: New York, 1978; Vol. III, p 225.
(10) Canters, G. W.; van Der Waals, J. H. In "The Porphyrins"; Dolphin, D., Ed.; Academic Press: New York, 1978; Vol. III, p 531.
(11) Stephens, P. J.; Suëtaak, W.; Schatz, P. N. *J. Chem. Phys.* **1966**, *44*, 4592.
(12) McHugh, A. J.; Gouterman, M.; Weiss, C. *Theor. Chim. Acta* **1972**, *24*, 346.
(13) Michl, J. *J. Am. Chem. Soc.* **1978**, *100*, 6801.
(14) Michl, J. *J. Am. Chem. Soc.* **1978**, *100*, 6812.
(15) Platt, J. R. *J. Chem. Phys.* **1949**, *17*, 484.
(16) Simpson, W. T. *J. Chem. Phys.* **1949**, *17*, 1218.
(17) Moffitt, W. *J. Chem. Phys.* **1954**, *22*, 320.
(18) We follow Gouterman's approximation of a porphyrin as a [16] annulene dianion,[2] rather than Michl's approximation as a [20] annulene dication.[13]

complex conjugate components receive + and − labels. Choosing the axis system as on top of Figure 1, one has

$$|e_{4u,c}\rangle = 2^{-3/2}\sum_{m=0}^{15}\cos(m\pi/2)|\chi_m\rangle$$

$$|e_{4u,s}\rangle = 2^{-3/2}\sum_{m=0}^{15}\sin(m\pi/2)|\chi_m\rangle$$

$$|e_{5g,c}\rangle = 2^{-3/2}\sum_{m=0}^{15}\cos(5m\pi/8)|\chi_m\rangle$$

$$|e_{5g,s}\rangle = 2^{-3/2}\sum_{m=0}^{15}\sin(5m\pi/8)|\chi_m\rangle$$

$$|e_{4u,\pm}\rangle = 1/4\sum_{m=0}^{15}\exp(\pm im\pi/2)|\chi_m\rangle$$

$$|e_{5g,\pm}\rangle = 1/4\sum_{m=0}^{15}\exp(\pm 5im\pi/8)|\chi_m\rangle \quad (1)$$

where the $|\chi_m\rangle$ functions are Löwdin-orthogonalized atomic orbitals, consisting of p_z-type functions on the perimeter. Table I summarizes the symmetry behavior of the components under the generators of D_{16h}.

The ground state, $|G\rangle$, has a closed shell structure $...(e_{4u})$.[4] The first excitation, $e_{4u} \rightarrow e_{5g}$, gives rise to two singlet states,[19] $^1E_{1u}$ and $^1E_{7u}$, which are related respectively to the intense Soret transition in the UV region and to the weak Q-labeled transition in the visible. In eq 2 the corresponding state functions have been defined in a way which conforms to the standard symmetry relations in Table I

$$|^1E_{1u,c}\rangle = 2^{-1/2}[(4c \rightarrow 5c)^1 + (4s \rightarrow 5s)^1]$$

$$|^1E_{1u,s}\rangle = 2^{-1/2}[(4c \rightarrow 5s)^1 - (4s \rightarrow 5c)^1]$$

$$|^1E_{7u,c}\rangle = 2^{-1/2}[(4c \rightarrow 5c)^1 - (4s \rightarrow 5s)^1]$$

$$|^1E_{7u,s}\rangle = 2^{-1/2}[-(4c \rightarrow 5s)^1 - (4s \rightarrow 5c)^1] \quad (2)$$

where $(4c \rightarrow 5c)^1$ symbolizes the singlet determinantal combination $2^{-1/2}(|e_{4u,c}e_{4u,s}\bar{e}_{4u,s}\bar{e}_{5g,c}| - |\bar{e}_{4u,c}e_{4u,s}\bar{e}_{4u,s}e_{5g,c}|)$ etc. (Bars symbolize spin $-1/2$). Complex components are most easily[13] defined as

$$|^1E_{1u,\pm}\rangle = (\pm 4 \rightarrow \pm 5)^1$$

$$|^1E_{7u,\pm}\rangle = (\pm 4 \rightarrow \mp 5)^1 \quad (3)$$

where again $(+4 \rightarrow +5)^1$ is a shorthand notation for a singlet determinant function $2^{-1/2}(|e_{4u,+}e_{4u,-}\bar{e}_{4u,+}\bar{e}_{5g,+}| - |\bar{e}_{4u,+}e_{4u,-}\bar{e}_{4u,-}e_{5g,+}|)$ etc. The functions in eq 3 also obey the conventions in Table I. They are related to the real components in eq 2 by the following relationships

$$|^1E_{1u,\pm}\rangle = -2^{-1/2}(|^1E_{1u,c}\rangle \pm i|^1E_{1u,s}\rangle)$$

$$|^1E_{7u,\pm}\rangle = -2^{-1/2}(|^1E_{7u,c}\rangle \pm i|^1E_{7u,s}\rangle) \quad (4)$$

(b) D_{4h} Functions. Substitution of the carbon atoms on the x and y axes by nitrogen atoms and addition of four external ethylene bridges to complete the pyrrole rings turns the cyclic perimeter into a porphyrin chromophore with D_{4h} symmetry. The e_{4u} representation, which is bipartite[20] in D_{16h}, thereby splits into two nondegenerate representations a_{1u} and a_{2u}; the nonbipartite e_{5g} level subduces an e_g representation, with components $e_{g,x}$ and $e_{g,y}$, which are properly defined in Table II. The D_{16h} states, $^1E_{1u}$ and $^1E_{7u}$, both become ^1E_u states in D_{4h}. Suitable zeroth-order functions for the HOMO and LUMO of D_{4h} metalloporphyrins may naturally be found by tetragonal projection of the cyclic orbitals in eq 1. *Instead Gouterman uses the four HOMO and LUMO functions, which result from direct LCAO–MO calculations on the porphin dianion.* These orbitals will be denoted $|a_{1u}\rangle$, $|a_{2u}\rangle$, $|e_{g,x}\rangle$, and $|e_{g,y}\rangle$. The accepted phase conventions,[2] which go with these ket symbols, are schematically presented in Figure 1 (bottom). Obviously the four orbitals of the Gouterman model still resemble the tetragonal components of e_{4u} and e_{5g}, *but the LCAO coefficients have been changed with respect to eq 1 so that the symmetry of the Gouterman orbital basis set no longer exceeds* D_{4h}. A correlation between the nodal pattern and phase conventions of the D_{16h} and D_{4h} basis set is expressed in eq 5.

$$|e_{4u,c}\rangle \rightarrow |a_{2u}\rangle$$

$$|e_{4u,s}\rangle \rightarrow -|a_{1u}\rangle$$

$$|e_{5g,c}\rangle \rightarrow |e_{g,x}\rangle$$

$$|e_{5g,s}\rangle \rightarrow |e_{g,y}\rangle \quad (5)$$

The minus sign, which goes with $|a_{1u}\rangle$, is a mere consequence of different phase conventions in the cyclic perimeter (eq 1) and the Gouterman (Figure 1) treatment. The $a_{1u} \rightarrow e_g$ and $a_{2u} \rightarrow e_g$ excitations both give rise to a ^1E_u state. Electron interaction causes these singlet transitions to mix. If both excitations were strictly degenerate, configuration interaction would yield the following linear combinations.

$$|B_x^0\rangle = 2^{-1/2}[(a_{2u} \rightarrow e_{g,x})^1 - (a_{1u} \rightarrow e_{g,y})^1]$$

$$|B_y^0\rangle = 2^{-1/2}[(a_{2u} \rightarrow e_{g,y})^1 + (a_{1u} \rightarrow e_{g,x})^1]$$

$$|Q_x^0\rangle = 2^{-1/2}[(a_{2u} \rightarrow e_{g,x})^1 + (a_{1u} \rightarrow e_{g,y})^1]$$

$$|Q_y^0\rangle = 2^{-1/2}[(a_{2u} \rightarrow e_{g,y})^1 - (a_{1u} \rightarrow e_{g,x})^1] \quad (6)$$

where B and Q are the traditional symbols for the excited states, associated with the strong UV bands (B) and the weak visible bands (Q). The component labels x and y strictly follow the conventions in Table II. Alternatively one could define + and − components, following the usual convention for the complex vectorial representation.

$$|B_\pm^0\rangle = (2)^{-1/2}(\mp|B_x^0\rangle - i|B_y^0\rangle)$$

$$|Q_\pm^0\rangle = (2)^{-1/2}(\mp|Q_x^0\rangle - i|Q_y^0\rangle) \quad (7)$$

Clearly the states in eq 6 and 7 can be related to the parent $^1E_{1u}$ and $^1E_{7u}$ states of the perimeter model. By combining the orbital correlations of eq 5 with the D_{16h} state functions (eq 2–4), one obtains the following state correlations.

$$|^1E_{1u,c}\rangle \rightarrow |B_x^0\rangle;\ |^1E_{1u,s}\rangle \rightarrow |B_y^0\rangle$$

$$|^1E_{7u,c}\rangle \rightarrow |Q_x^0\rangle;\ |^1E_{7u,s}\rangle \rightarrow -|Q_y^0\rangle$$

$$|^1E_{1u,+}\rangle \rightarrow |B_+^0\rangle;\ |^1E_{1u,-}\rangle \rightarrow -|B_-^0\rangle$$

$$|^1E_{7u,+}\rangle \rightarrow -|Q_-^0\rangle;\ |^1E_{7u,-}\rangle \rightarrow |Q_+^0\rangle \quad (8)$$

The minus sign in the expression for $|Q_y^0\rangle$ and the +/− inversion in the correlation $E_{7u,\pm} \rightarrow Q_\mp^0$ stems from the symmetry adaptation of the E_{7u} components to the D_{4h} convention in Table II. The equation clearly demonstrates that *the zeroth-order states of the "4-orbital" model are constructed from* D_{16h} *coupling coefficients, translated into the phase conventions of Table II.* If the two constituent single excitations cease to be strictly degenerate this rigorous coupling scheme will be perturbed and B–Q mixing becomes allowed, as indicated below.

$$|B_i\rangle = (\cos\nu)|B_i^0\rangle + (\sin\nu)|Q_i^0\rangle$$

$$|Q_i\rangle = -(\sin\nu)|B_i^0\rangle + (\cos\nu)|Q_i^0\rangle \quad (9)$$

where i may stand for any component label x, y, +, or −. The mixing coefficient ν is defined by eq 10 and the resulting state energies are expressed as in eq 11. In these equations three

$$\tan 2\nu \equiv A_{1g}/A_{1g}'';\ -\pi/2 \leq 2\nu \leq \pi/2 \quad (10)$$

$$E(B) = A_{1g}' + A_{1g}''/\cos 2\nu \quad (11a)$$

$$E(Q) = A_{1g}' - A_{1g}''/\cos 2\nu \quad (11b)$$

(19) In many references the $^1E_{7u}$ state is labeled erroneously as a $^1E_{9u}$.
(20) Ceulemans, A. *Chem. Phys.* **1982**, *66*, 169.

characteristic empirical parameters of Gouterman's model are introduced.[1] A_{1g}' represents the center of gravity of the two single excitations $a_{1u} \rightarrow e_g$ and $a_{2u} \rightarrow e_g$. The energy distance $E(B^0) - E(Q^0)$ between the zeroth-order states is given by $2A_{1g}''$. The Soret state being the upper level, A_{1g}'' is bound to be positive. The remaining parameter A_{1g} stands for the interaction element between B^0 and Q^0. This is the parameter which is responsible for B–Q mixing. As can be seen from eq 12, $2A_{1g}$ corresponds to the configurational splitting of the two single excitations.

$$A_{1g} = 1/2[E(a_{2u} \rightarrow e_g) - E(a_{1u} \rightarrow e_g)] \quad (12)$$

If both configurations are assumed to have similar interelectronic repulsion energies the latter parameter may be approximated as the energy difference of the two HOMO levels:

$$A_{1g} \approx 1/2[\epsilon(a_{1u}) - \epsilon(a_{2u})] \quad (13)$$

It must be kept in mind that A_{1g}, and hence ν, is a signed quantity. A_{1g}'' being positive, ν and A_{1g} will always have the same sign, this is positive if $\epsilon(a_{1u}) > \epsilon(a_{2u})$ and negative if $\epsilon(a_{1u}) < \epsilon(a_{2u})$.

The energy order of the a_{1u} and a_{2u} HOMO's and hence the sign of ν varies with ring substituents, central metal character, and axial ligation in a predictable way, which is dictated by the orbital nodal characteristics.[22] As an example only the a_{2u} orbital has electron density at the meso positions so that *meso*-phenyl substituents should cause its energy to rise relative to the a_{1u} orbital. On the other hand, a_{2u} has little density at the exo positions as compared to the a_{1u} partner so that *exo*-alkyl groups are anticipated to induce a HOMO splitting of opposite sign. The resulting increase in ν in going from a *meso*-phenyl ring to an *exo*-alkyl ring will be studied experimentally in section III. This section will also include a discussion of the ν-monitoring role of the axial ligands.

If we now compare the final state functions in D_{16h} and D_{4h}, *two different ways of modelling the symmetry lowering can clearly be distinguished*: in the first place, one has to describe the "metamorphosis" of the orbital basis set itself, as expressed in eq 5. In the second place, one has to account for the departure of the high-symmetry coupling limit, as given in eq 9. Both effects will influence the evaluation of moment integrals.

(c) Moment Integrals. In D_{4h} the orbital transitions $a_{1u} \rightarrow e_g$ and $a_{2u} \rightarrow e_g$ will be polarized in the porphyrin plane. Gouterman[1] introduces two parameters R_{1y} and R_{2y} to describe the corresponding transition moment lengths in the y direction. Generalizing these results to x and y directions, one has

$$R_1 = \langle (a_{1u} \rightarrow e_{g,x})^1|y|G\rangle = -\langle (a_{1u} \rightarrow e_{g,y})^1|x|G\rangle$$

$$R_2 = \langle (a_{2u} \rightarrow e_{g,y})^1|y|G\rangle = \langle (a_{2u} \rightarrow e_{g,x})^1|x|G\rangle \quad (14)$$

With the conventional choice of orbital phases (see Figure 1) both parameters will be positive. The transition moment lengths for the zeroth- and first-order biconfigurational transitions then become

$$\langle B_k^0|k|G\rangle = 2^{-1/2}(R_1 + R_2) \equiv R$$

$$\langle Q_k^0|k|G\rangle = 2^{-1/2}(R_2 - R_1) \equiv r$$

$$\langle B_k|k|G\rangle = R \cos \nu + r \sin \nu$$

$$\langle Q_k|k|G\rangle = -R \sin \nu + r \cos \nu \quad (15)$$

where k stands for x or y. Obviously similar formula's involving the complex state functions may be derived by straightforward combination of eq 7, 9, and 15. A crude estimate[1] of the parameters R and r using the Longuet–Higgins D_{4h} basis orbitals[21] gives $R = 2.9$ Å, $r = 0.07$ Å. These values are comparable with $R = 3.59$ Å, $r = 0.0$ Å, which may be calculated from Michl's expressions applied to D_{16h} orbitals. The zero value of the r parameter in the cyclic polyene limit reflects the symmetry selection rule for the corresponding $^1A_{1g} \rightarrow {}^1E_{7u}$ transition. In contrast the Gouterman model allows for a small but nonvanishing value of r. This must be looked upon as a typical consequence of the use of four basis orbitals, whose symmetry does not exceed D_{4h}.

As far as the angular momentum parameters are concerned we will only investigate matrix elements in ℓ_z since these are the only Zeeman terms which may couple with the in-plane polarized electric transition moments. Relevant parameters for the angular momenta of the single configurational states may be defined as in eq 16. In a frozen orbital approximation, which is the usual working hypothesis of the Gouterman model, these parameters reduce to the orbital elements $L_1 = i\langle a_{1u}|\ell_z|a_{2u}\rangle$, $L_2 = L_2' = i\langle e_{g,x}|\ell_z|e_{g,y}\rangle$. In the conventional phase choice (see Figure 1) all these parameters will be real and positive. Angular momenta of the final excited states then can be expressed as follows:

$$L_1 = i\langle (a_{1u} \rightarrow e_{g,k})^1|\ell_z|(a_{2u} \rightarrow e_{g,k})^1\rangle,\ k = x, y$$

$$L_2 = i\langle (a_{1u} \rightarrow e_{g,x})^1|\ell_z|(a_{1u} \rightarrow e_{g,y})^1\rangle$$

$$L_2' = i(a_{2u} \rightarrow e_{g,x})^1|\ell_z|(a_{2u} \rightarrow e_{g,y})^1\rangle \quad (16)$$

$$\langle B_\pm^0|\ell_z|B_\pm^0\rangle = \pm(-L_1 + 1/2(L_2 + L_2')) \equiv \pm\ell$$

$$\langle Q_\pm^0|\ell_z|Q_\pm^0\rangle = \pm(L_1 + 1/2(L_2 + L_2')) \equiv \pm L$$

$$\langle B_\pm|\ell_z|B_\pm\rangle = \pm\ell \cos^2 \nu \pm L \sin^2 \nu$$

$$\langle Q_\pm|\ell_z|Q_\pm\rangle = \pm\ell \sin^2 \nu \pm L \cos^2 \nu \quad (17)$$

Zeeman mixing between the UV and VIS bands is given by

$$\langle B_\pm|\ell_z|Q_\pm\rangle = \pm(L - \ell)\sin\nu \cos \nu \pm \tfrac{1}{2}(L_2' - L_2) \quad (18)$$

In eq 18 the first term in ν reflects the deviation of the D_{16h} coupling scheme, while the second term stems from a relaxation of the frozen orbital approximation. In all probability the latter term will be negligible unless ν is very close to zero. Hence in the subsequent treatment the term in ν will be considered to be the main mechanism of off-diagonal Zeeman mixing.

Estimates of ℓ and L do not point to qualitative differences between D_{16h} and D_{4h} schemes, because in both cases ℓ and L are symmetry allowed. Using Michl's cyclic perimeter functions[13] one obtains $L = 6.24\hbar$, $\ell = 0.09\hbar$, to be compared with extended Hückel results $L = 4.76\ \hbar$, $\ell = 0.02\hbar$. More elaborate Pariser–Parr–Pople calculations by McHugh et al.[12] suggest a slightly negative value for ℓ in unsubstituted porphine. This could give rise to anomalous or inverted MCD spectra in the Soret region, but such effect has not been observed in ordinary metalloporphyrins (see, however, ref 22 and 23).

II. Evaluation of the MCD Parameters

(a) Parametric MCD Expressions. Calculations of the Faraday parameters will be based entirely on the general MCD formulas presented by Piepho and Schatz in their recent monograph.[24] These authors follow the conventions introduced by Stephens[25] in 1976. To emphasize the difference with previous conventions they advocate the use of modified symbols $\mathcal{D}_0$, $\mathcal{A}_1$, $\mathcal{B}_0$, $\mathcal{C}_0$ instead of the previous notation D for dipole strength and A, B, and C for MCD parameters. Orientationally averaged parameters, which apply for a collection of randomly oriented molecules in solution, are denoted by a bar: $\bar{\mathcal{D}}_0$, $\bar{\mathcal{A}}_1$, $\bar{\mathcal{B}}_0$, and $\bar{\mathcal{C}}_0$. For the particular case of a three-state system, consisting of $^1A_{1g}$ ground state, G, and two excited singlet states of E_u symmetry, J and J', the general

(21) Longuet-Higgins, H. C.; Rector, C. W.; Platt, J. R. *J. Chem. Phys.* **1950**, *18*, 1174.

(22) Keegan, J. D.; Stolzenberg, A. M.; Lu, Y.-C.; Linder, R. E.; Barth, G.; Moscowitz, A.; Bunnenberg, E.; Djerassi, C. *J. Am. Chem. Soc.* **1982**, *104*, 4305, 4317.

(23) Djerassi, C.; Lu, Y.; Waleh, A.; Shu, A. Y. L.; Goldbeck, R. A.; Kehres, L. A.; Crandell, C. W.; Wee, A. G. H.; Knierzinger, A.; Gaete-Holmes, R.; Loew, O. H.; Clezy, P. S.; Bunnenberg, E. *J. Am. Chem. Soc.* **1984**, *106*, 4241.

(24) Piepho, S. B.; Schatz, P. N. "Group Theory in Spectroscopy"; Wiley: New York, 1983.

(25) Stephens, P. J. *Adv. Chem. Phys.* **1976**, *35*, 197.

expressions (ref 24, p 88) reduce to the simple formulas given in eq 19:

$$\bar{\mathcal{D}}_0(G \rightarrow J) = (2/3)|\langle G|-ex|Jx\rangle|^2$$

$$\bar{\mathcal{A}}_1(G \rightarrow J) = \langle J+|\ell_z|J+\rangle\, \bar{\mathcal{D}}_0(G \rightarrow J)$$

$$\bar{\mathcal{B}}_0(G \rightarrow J) = -\frac{4\langle J+|\ell_z|J'+\rangle\, \langle G|-ex|Jx\rangle\, \langle J'y|-ey|G\rangle}{3(E(J') - E(J))} \qquad (19)$$

where $-e$ is the electron's charge ($e \approx 4.8$ D Å^{-1}). $\bar{\mathcal{D}}_0$ is in units of square Debye. Units for the $\bar{\mathcal{A}}_1$ term are $\hbar$ (Debye)^2. $\bar{\mathcal{B}}_0$ is expressed in units of $\hbar$ D^2/cm^{-1}. Upon substitution of eq 15 and 17 into eq 19 we finally obtain the desired parametric expressions for the magnetooptical properties of D_{4h} porphyrins in the framework of the Gouterman model.

$$\bar{\mathcal{D}}_0(G \rightarrow B) = (2e^2/3)(R \cos \nu + r \sin \nu)^2$$

$$\bar{\mathcal{A}}_1(G \rightarrow B) = (\ell \cos^2 \nu + L \sin^2\nu)\bar{\mathcal{D}}_0(G \rightarrow B)$$

$$\bar{\mathcal{B}}_0(G \rightarrow B) = -\frac{e^2(L - \ell)((R^2 - r^2) \sin^2 2\nu - Rr \sin 4\nu)}{3(E(B) - E(Q))} \qquad (20)$$

$$\bar{\mathcal{D}}_0(G \rightarrow Q) = (2e^2/3)(-R \sin \nu + r \cos \nu)^2$$

$$\bar{\mathcal{A}}_1(G \rightarrow Q) = (\ell \sin^2 \nu + L \cos^2\nu)\bar{\mathcal{D}}_0(G \rightarrow Q)$$

$$\bar{\mathcal{B}}_0(G \rightarrow Q) = -\bar{\mathcal{B}}_0(G \rightarrow B) \qquad (21)$$

(b) Discussion. A discussion of these expressions will focus on the distinct roles of the mixing coefficient ν and the transition moment length r, which represent two different mechanisms to promote the intensity of the Q band. A convenient starting point is the D_{16h} limit, where both mechanisms are symmetry forbidden. Accordingly in D_{16h} both r and ν are equal to zero, while the other integrals L, ℓ, and R are symmetry allowed and may adopt typical cyclic perimeter values. As a result only the Soret band will carry electric dipole intensity. Its MCD signal will consist of a weak isolated A term, with the same sign as ℓ. No Zeeman mixing between Q and B transitions will be allowed.

The introduction of a non-zero value for ν while keeping all moment parameters unaltered corresponds to a relaxation of the high-symmetry coupling conditions, without changing the nature of the basis orbitals. Via this mechanism the Q band acquires some B-band character and vice versa. The MCD expressions for such a perturbed two-state system have been worked out by Michl.[13] The Faraday parameters D, A, and B in Michl's convention are related to the present formalism in the following way:

$$D = 3\bar{\mathcal{D}}_0$$

$$A/D = (\beta_e/2\hbar)\bar{\mathcal{A}}_1/\bar{\mathcal{D}}_0$$

$$B = -(3\beta_e/2\hbar)\bar{\mathcal{B}}_0 \qquad (22)$$

where β_e is the Bohr magneton. The factor $\beta_e/\hbar$ procures the conversion of the $\hbar$ unit for angular momenta into the β_e unit for magnetic momenta. By combining eq 22 with the appropriate translation of nomenclature,[26] Michl's result can be shown to coincide exactly with a special solution of eq 20 and eq 21, *in which the r parameter has been put equal to zero.* This is indeed the logical outcome of a first-order perturbational treatment in a functional space of D_{16h} symmetry. In this approximation one predicts for both bands normal A terms ($\bar{\mathcal{A}}_1 > 0$) and nonvanishing B terms of opposite sign. Since $L > \ell$ and $E(B) > E(Q)$ the $\bar{\mathcal{B}}_0(G \rightarrow Q)$ parameter is expected to be *positive, irrespective of the sign of* ν. In Figure 2 we have plotted the three weakly allowed terms, $\bar{\mathcal{D}}_0(G \rightarrow Q)$, $\bar{\mathcal{B}}_0(G \rightarrow Q)$, and $(\bar{\mathcal{A}}_1/\bar{\mathcal{D}}_0)(G \rightarrow B)$, as a function of the mixing coefficient ν. All three curves resemble parabolic wells. The dipole strength and B term of the Q band are tangent to the ν axis in the coordinate origin, since the Q band becomes forbidden for $\nu = 0$. For $L > \ell$ the angular momentum

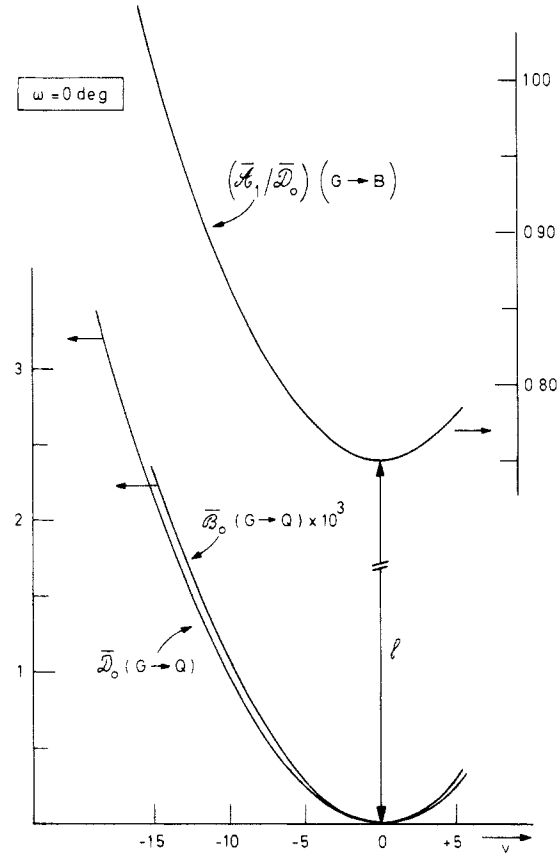

Figure 2. Influence of Q–B mixing on the weakly allowed MCD quantities, according to the Michl approximation (see ref 13). The figure displays $\bar{\mathcal{A}}_1/\bar{\mathcal{D}}_0$ for the B band and $\bar{\mathcal{D}}_0$ and $\bar{\mathcal{B}}_0$ for the Q band, as a function of the Q–B mixing coefficient ν, defined in eq 9. The Michl treatment is marked by a zero dipole moment integral r for the Q^0 state. Likewise the pivot angle ω equals zero (cf. eq 24). Other parameters adopt typical values for the ZnOEP series: $R = 1.45$ Å, $L = 4.65\hbar$, $\ell = 0.75\hbar$, $E(B) - E(Q) = 6900$ cm^{-1}. The mixing coefficient ν is expressed in degrees; units for the MCD quantities are given in the text (see eq 19).

of the Soret state, expressed as $\bar{\mathcal{A}}_1/\bar{\mathcal{D}}_0$, will increase as a function of $\sin^2 \nu$, while the angular momentum of the Q state will be quenched to the same extent (see eq 23). Plotted on a ν axis these quantities reach extreme values for $\nu = 0$.

$$(\bar{\mathcal{A}}_1/\bar{\mathcal{D}}_0)(G \rightarrow B) = \ell + (L - \ell) \sin^2 \nu$$

$$(\bar{\mathcal{A}}_1/\bar{\mathcal{D}}_0)(G \rightarrow Q) = L - (L - \ell) \sin^2 \nu \qquad (23)$$

The effect of introducing a non-zero value of r is shown in Figure 3. First of all the figure shows that the $(\bar{\mathcal{A}}_1/\bar{\mathcal{D}}_0)(G \rightarrow B)$ term (see eq 23) does not change if r deviates from zero. As for the dipole strength and B term of the Q band one may note slight changes in the shapes of the parabolic wells, but more importantly, the figure also shows relative displacements of the functions as a whole. The point of vanishing dipole strength is shifted horizontally over an angle ω, defined in eq 24. Since R is always positive

$$\tan \omega = r/R \qquad \text{with } -\pi/4 \leq \omega \leq \pi/4 \qquad (24)$$

the signs of ω and r will coincide. The ratio of the dipole strengths of B and Q bands can be expressed as a simple function of ν and ω.

$$\bar{\mathcal{D}}_0(G \rightarrow Q)/\bar{\mathcal{D}}_0(G \rightarrow B) = \tan^2 (\nu - \omega) \qquad (25)$$

Hence in contrast to the case where r equals zero, *the measurement of the relative dipole strengths does not yield absolute coordinate points on the* ν *axis, but only relative displacements from the pivot point* $\nu = \omega$.

The parabolic well $\bar{\mathcal{B}}_0(G \rightarrow Q)$ is shifted over only half the distance of the $\bar{\mathcal{D}}_0(G \rightarrow Q)$ well, but at the same time it is

(26) One has: $\ell = -\mu^-\hbar/\beta_e$, $L = -\mu^+\hbar/\beta_e$; μ^- and μ^+ symbolize the magnetic moments of the parent $^1E_{1u}$ and $^1E_{7u}$ states. In ref 13, p 6806, the formula $\tan 2\alpha = 2|a|/(B - L)$ which is the equivalent of the present eq 10, should read $\tan 2\alpha = 2a/(B - L)$.

Table III. Absorption and MCD Spectral Data[a] for ZnTPP and ZnOEP[b] in Noncoordinating Solvents and with Pyridine and Cyanide as Axial Ligands

	Q(0,0) band					Q(0,1) band			B(0,0) band				
	$\mathcal{E}_{max}$	(ϵ_{max})	$\bar{\mathcal{D}}_0$	$\bar{\mathcal{A}}_1/\bar{\mathcal{D}}_0$	$10^4\bar{\mathcal{B}}_0$	$\mathcal{E}_{max}$	(ϵ_{max})	$\bar{\mathcal{D}}_0$	$\mathcal{E}_{max}$	(ϵ_{max})	$\bar{\mathcal{D}}_0$	$\bar{\mathcal{A}}_1/\bar{\mathcal{D}}_0$	
ZnTPP	17010	(3865)	0.42	2.48	11	18230	(23845)	3.16	23715	(571150)	50.66	0.73	*c*
	16950	(3450)	0.32	3.52	14		(23000)				53.33		*d*
	17000					18200			23670				*e*
ZnTPP(py)	16620	(10530)	1.09	3.47	38	17790	(23160)	2.94	23310	(702000)	51.50	0.76	*c*
	16610	(10360)	1.09	3.22	22		(22040)				57.36		*d*
	16610					17790			23350				*e*
ZnTPP(CN)	16100	(19200)	2.12	3.07	69	17295	(18230)	2.42	22782	(684775)	46.77	0.94	*c*
	16170					17340			22800				*e*
ZnOEP	17600	(30610)	2.27	4.39	0.0	18820	(17130)	2.04	24785	(356000)	33.05	0.82	*c*
	17650	(39300)	2.13	3.03		18925	(16000)						*f*
	17480	(24500)				18655	(18200)		24570	(416870)			*g*
	17600					18800			24700				*h*
ZnOEP(py)	17310	(19100)	1.40	4.87	−14	18450	(22030)	2.66	24120	(432740)	31.60	0.75	*c*
	17315	(16700)	1.33	3.90		18445	(17650)						*f*
ZnOEP(CN)	16945	(10210)	0.59	3.98	−24	18050	(21160)	2.56	23447	(418670)	25.88	0.81	*c*

[a] $\mathcal{E}_{max}$ refers to the energy of the band maximum (in cm^{-1}) and ϵ_{max} is the corresponding molar extinction coefficient (in L mol^{-1} cm^{-1}). $\bar{\mathcal{D}}_0$, $\bar{\mathcal{A}}_1$, and $\bar{\mathcal{B}}_0$ are the orientationally averaged Faraday parameters in the Schatz–Piepho convention.[24] Theoretical expressions and units for these parameters are given in the text (see eq 19). [b] Ligand abbreviations: TPP = tetraphenylporphyrine, OEP = octaethylporphyrine, py = pyridine. [c] This work. Spectra taken in dry benzene. [d] Reference 27; solvent = toluene. [e] Reference 5, ZnTPP and ZnTPP(CN) in benzene, ZnTPP(py) in toluene. [f] Reference 28, ZnOEP in *n*-octane, ZnOEP(py) in EPA-py. [g] Reference 29, solvent = dioxane. [h] Reference 6, solvent = toluene.

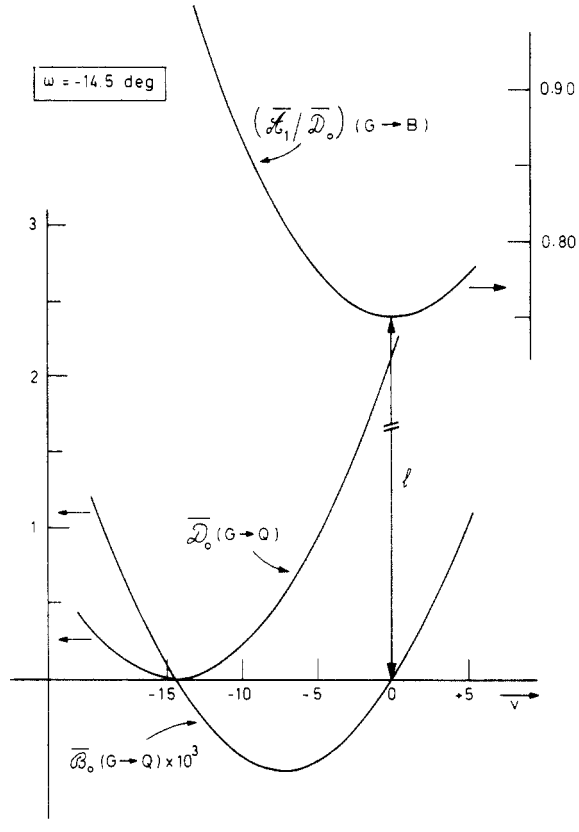

Figure 3. Influence of Q–B mixing on the weakly allowed MCD quantities according to the Gouterman model. This model differs from the Michl approximation, shown in Figure 2, by a non-zero value for the intrinsic transition dipole moment r of the G → Q^0 excitation. The curves were drawn using r = −0.375 Å, or ω = −14.5° as is the case for ZnOEP (see Table IV). Other parameters are the same as in Figure 2. From a comparison of Figure 2 and Figure 3 one may conclude that the r parameter only affects the $\bar{\mathcal{D}}_0$ and $\bar{\mathcal{B}}_0$ quantities. In Figure 3 the $\bar{\mathcal{D}}_0$ curve is displaced horizontally over an angle ω. The $\bar{\mathcal{B}}_0$ curve is shifted over an angle $\omega/2$ and adopts negative values inside the interval $[\omega,0]$.

vertically displaced toward negative $\bar{\mathcal{B}}_0$ values. The resulting curve intersects the ν axis at angles ω and 0 and reaches a minimum at $\nu = \omega/2$. Outside the interval $[\omega,0]$ the $\bar{\mathcal{B}}_0$ parameter of the Q band remains positive, in qualitative agreement with the predictions of Michl's first-order perturbational model. However, inside the interval $[\omega,0]$ $\bar{\mathcal{B}}_0$(G → Q) will be negative. Likewise $\bar{\mathcal{B}}_0$(G → B) will adopt an anomalous positive sign in the same interval.

Table IV. Model Parameters for the ZnTPP and ZnOEP Series[a]

	A_{1g}' (cm^{-1})	$R^2 + r^2$ (Å²)	$L + \ell$ ($\hbar$)	$\lvert\nu - \omega\rvert$ (deg)
ZnTPP	20360	3.32	3.21	5.2
ZnTPP(py)	19965	3.42	4.23	8.3
ZnTPP(CN)	19440	3.18	4.01	12.0
ZnOEP	21190	2.30	5.21	14.7
ZnOEP(py)	20715	2.15	5.62	11.9
ZnOEP(CN)	20195	1.72	4.79	8.6

[a] The parameters were extracted from the spectral data, obtained in this work (see Table III). Parameter definitions are given in eq 11, 25, and 27.

In conclusion, the $r \neq 0$ premise of the Gouterman model substantially modifies the predictions from a first-order perturbational model. For values of the mixing coefficient ν between 0 and ω one expects an anomalous negative sign for the MCD parameter $\bar{\mathcal{B}}_0$(G → Q) and an opposite ν dependence of the dipole strength of the Q band and the angular momentum of the Soret band: $\bar{\mathcal{D}}_0$(G → Q) reaches its minimum for $\nu = \omega$ while $(\bar{\mathcal{A}}_1/\bar{\mathcal{D}}_0)$(G → B) is minimal in the coordinate origin $\nu = 0$. Outside this interval the $\bar{\mathcal{B}}_0$(G → Q) parameter is always positive and both $\bar{\mathcal{D}}_0$(G → Q) and $(\bar{\mathcal{A}}_1/\bar{\mathcal{D}}_0)$(G → B) show a similar ν dependence, exactly as predicted in Michl's treatment. Comparison with other theoretical studies[11,12] of the MCD of metalloporphyrins could not be pursued since these studies did not present detailed parametric expressions for all the MCD terms in the degenerate D_{4h} case. In the final section the predicted changes of the MCD signal with a change in coupling conditions will be confronted with existing and newly obtained experimental spectra.

III. Comparison with Experiment

In Tables III and IV we present spectral data for two series of substituted Zn porphyrins with varying axial ligands. These data were obtained by using the experimental procedures described below. Where possible literature data have been included for comparison.[5,6,27-29] Throughout the Schatz–Piepho conventions

(27) Keegan, J. D.; Bunnenberg, E.; Djerassi, C. *Spectrochim. Acta A* **1984**, *40*, 287.

have been used. Conversion formulas to Michl's convention are given in eq 22 (see also ref 24, p 539).

(a) Experimental Procedures. The compounds zinc tetraphenylporphyrin (ZnTPP) and zinc octaethylporphyrin (ZnOEP) were synthesized from the parent porphyrins (Aldrich and Sigma, respectively) by the method of Adler et al.[30] The precipitated products were recrystallized by slowly adding ethanol to a concentrated chloroform solution of the metalloporphyrins.[31] The vacuum-dried neat compounds were dissolved in benzene which had been dried over 4 Å molecular sieves. Axially substituted derivatives were made by adding to these solutions the minimum amount of free ligand (pyridine or Bu_4NCN) needed to form the five-coordinated complexes. Absorption spectra were recorded with a Cary 219 double-beam spectrophotometer. MCD measurements were performed on a Cary 61 CD spectropolarimeter, adapted for MCD with a 0.75 T electromagnet.

The extraction of the Faraday parameters requires the use of a curve-fitting method, which enables the deconvolution of the electronic origins (B(0,0) and Q(0,0)) and the vibronic satellites (B(0,1), Q(0,1), etc...). A simple Gaussian band analysis was adopted, based on the following expressions:[32]

$$\epsilon/\mathscr{E} = 326.6\sum_J \bar{\mathcal{D}}_0(\mathrm{G} \rightarrow \mathrm{J}) f^J(\mathscr{E})$$

$$\frac{[\theta]_M}{\mathscr{E}} = (5.029 \times 10^5) B \sum_J \left[\bar{\mathcal{A}}_1(\mathrm{G} \rightarrow \mathrm{J}) \left(-\frac{\delta f^J(\mathscr{E})}{\delta \mathscr{E}} \right) + \bar{\mathcal{B}}_0(\mathrm{G} \rightarrow \mathrm{J}) f^J(\mathscr{E}) \right] \quad (26)$$

where the summation runs over a basis set of Gaussian primitives; ϵ and $[\theta]_M$ respectively symbolize the molar extinction coefficient (in L mol^{-1} cm^{-1}) and the molar ellipticity (in deg cm^2 $dmol^{-1}$). B is the magnetic field (in T), $\mathscr{E}$ represents the energy coordinate (in cm^{-1}), and f is a normalized Gaussian line-shape function, $f = \Delta^{-1}\pi^{-1/2} \exp(-(\mathscr{E} - \mathscr{E}^0)^2/\Delta^2)$, with a bandwidth Δ and a frequency center $\mathscr{E}^0$.

A Gaussian resolution of the absorption spectra proved to be fairly straightforward. The $\bar{\mathcal{D}}_0$ values in the tables refer to the dipole strengths of the principal Gaussian components under the Q(0,0) and B(0,0) absorption maxima. Although the present model is not concerned with vibronic transitions, values for $\bar{\mathcal{D}}_0$(G → Q(0,1)) have also been listed for comparison with literature data.

The MCD spectrum of the Soret region essentially consists of one normal A term, which can easily be reproduced by a Gaussian line shape. Small subsidiary features may be accounted for by weak B terms, but these are less reliable as compared to the dominant A term and have not been included in Table III. The bandwidth of the A term appears to be somewhat less than the bandwidth of the absorption band. Frequency differences between $\mathscr{E}^0$ and $\mathscr{E}_{max}$ are barely significant. Finally there is a fair agreement between the results of a curve-fitting analysis and $\bar{\mathcal{A}}_1$(G → B) values obtained by the integration method of moment analysis.

The MCD spectra of the Q(0,0) region also seem to be dominated by a single normal A term, which is, however, visibly asymmetric. The band asymmetry may be attributed to an underlying B term, with opposite sign in the ZnTPP and ZnOEP series.

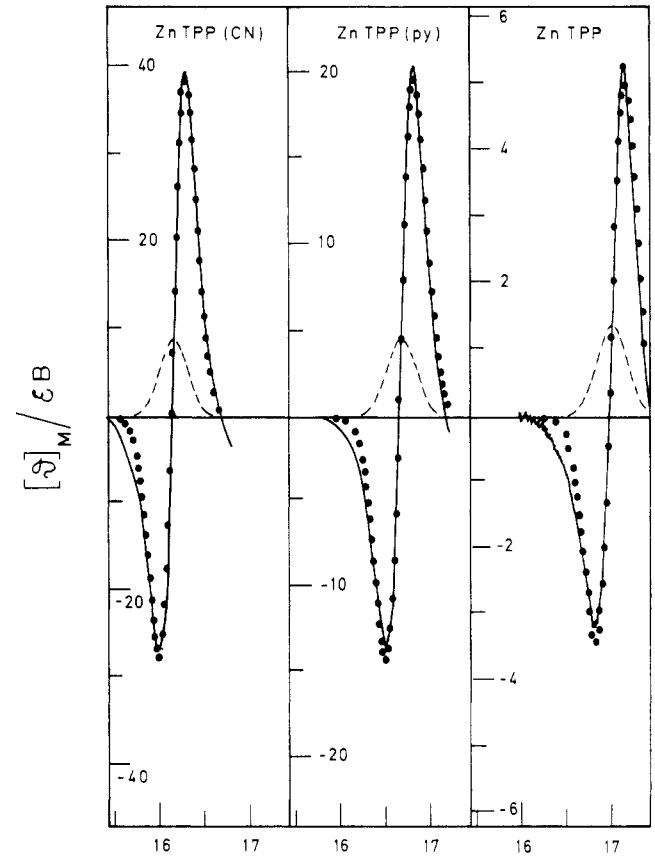

Figure 4. MCD spectra of the Q(0,0) band in zinc tetraphenylporphyrin and its pyridinate and cyanide complexes, taken in benzene solution. $[\theta]_M/\mathscr{E}B$ is the molar ellipticity (in deg cm^2/dmol) per unit wavenumber (in cm^{-1}) and per unit magnetic field (in T). The abscissa corresponds to wavenumbers in units of 1000 cm^{-1}. Full lines represent the experimental spectra. Dotted lines correspond to the calculated spectra, based on a Gaussian curve fitting analysis using eq 26. The fitting parameters $\bar{\mathcal{A}}_1$ and $\bar{\mathcal{B}}_0$ are resumed in Table II. The dashed lines display the isolated $\bar{\mathcal{B}}_0$ components of the Gaussian analysis. As can be seen from the figure, the simple Gaussian fitting procedure fails to reproduce the low-energy tails of the spectra. Nonetheless, the $\bar{\mathcal{B}}_0$ component is clearly positive and increases from ZnTPP to ZnTPP(CN).

In the Q(0,0) region of the ZnTPP compounds, which is displayed in Figure 4, one may note a large difference between the shapes of the left and right wings of the A term. In view of this lobe inequality the fitting performance of a simple Gaussian analysis is rather poor. Nonetheless it is clear from Figure 4 that the $\bar{\mathcal{B}}_0$(G → Q) component in the ZnTPP series will carry a positive sign.

In the Q(0,0) region of the ZnOEP compounds, which is shown in Figure 5, A and B terms can easily be resolved by Gaussian analysis. In spite of this neat resolution we obtain angular momenta for the Q state, which are considerably higher than the values in ref 28 (see Table III). High angular momenta for the Q state are not unusual though, as indicated for instance by the $\bar{\mathcal{A}}_1/\bar{\mathcal{D}}_0$(G → Q) ratio of 6.94 $\hbar$, which is reported for the closely related zinc hematoporphyrin.[11]

(b) Discussion. A multiparameter model owes its relevance to the observation of systematic trends in the properties of large series of closely related compounds. Ideal test cases are those series, which embody a variation of one single parameter at the time, all other parameters remaining approximately constant throughout the series. Such results most clearly visualize the functioning of each individual parameter in the framework of the model. In porphyrin spectroscopy the closest one may come to such a systematic unidimensional parameter variation is through gradually changing axial ligation on a fixed metallo-ring template.

(28) Barth, G.; Linder, R. E.; Bunnenberg, E.; Djerassi, C.; Seamans, L.; Moscowitz, A. *J. Chem. Soc., Perkin Trans. 2* **1974**, 1706.
(29) Buchler, J. W.; Kokisch, W.; Smith, P. D. *Struct. Bonding (Berlin)* **1978**, *34*, 79.
(30) Adler, A. D.; Longo, F. R.; Kampas, F.; Kim, J. *J. Inorg. Nucl. Chem.* **1970**, *32*, 2443.
(31) Dorough, G. D.; Miller, J. R.; Huennekens, F. M. *J. Am. Chem. Soc.* **1951**, *73*, 4315.
(32) Errata in the section on Gaussian analysis in ref 24: Figure 7.8.1 on p 149 represents $-f_G'(\mathscr{E})$ and not $f_G'(\mathscr{E})$; formula 7.8.10 should read

$$\left(\frac{\Delta A'}{\mathscr{E}}\right)_{\Delta/2^{1/2}} = \gamma \mathcal{A}_1 \left(\frac{\sqrt{2}}{\Delta^2\sqrt{\pi e}}\right) \mu_B B + \left(\frac{\Delta A'}{\mathscr{E}}\right)_0 e^{-1/2}$$

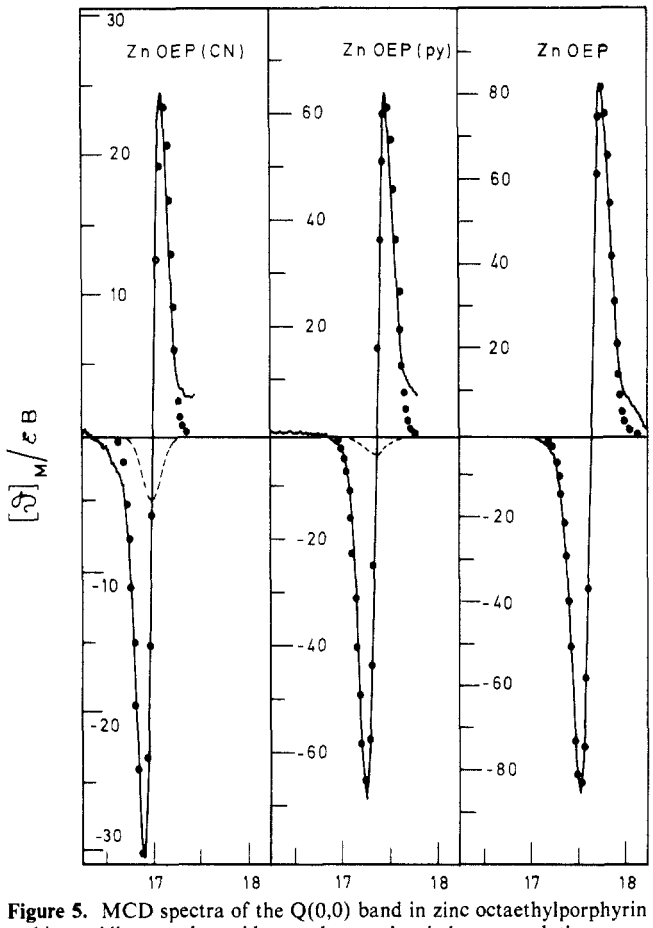

Figure 5. MCD spectra of the Q(0,0) band in zinc octaethylporphyrin and its pyridinate and cyanide complexes, taken in benzene solution; same conventions as in Figure 4. As can be seen from the figure, $\bar{\mathcal{B}}_0$ vanishes for ZnOEP and is negative in the py and CN complex.

Accordingly the role of the axial ligand will be the central theme of the subsequent discussion.

Electronic interactions between the optical orbitals of the porphyrin chromophore and an axial nucleophile are mediated by the valence orbitals of the metal.[29,33] Only two transmission paths are allowed: (i) The σ-donor level of the nucleophile may interact with the a_{2u} HOMO via the p_z-valence orbital on the metal. (ii) The π-donor and π-acceptor levels of the nucleophile may interact with the e_g LUMO's via the dπ-valence orbitals on the metal.

In contrast axial perturbation has no influence on the a_{1u} HOMO, since this HOMO has nodes on the pyrrolic nitrogens. In a post-transition-metal complex with a contracted d shell, the proposed d-mediated effect is not expected to be very important either. *This leaves the energy of the a_{2u} HOMO, as the only effective variable across an axial substitution series*: increasing σ-donor strength of the axial ligand in the sequence $C_6H_6 \rightarrow$ py $\rightarrow CN^-$ will lead to increasing destabilization of the a_{2u} HOMO.

Considering the Gouterman energy parameters A_{1g}, A_{1g}', and A_{1g}'', the increase of the a_{2u} orbital energy will induce a concomitant lowering of the average transition energy parameter A_{1g}' and of the HOMO splitting parameter A_{1g} (see eq 13). The two-electron parameter A_{1g}'' is not directly affected. Experimentally one may indeed observe a pronounced decrease of A_{1g}' in complexes with strong axial σ donors. Direct observation of a similar variation of A_{1g} is seriously handicapped by the fact that the frequencies of Soret and Q band are not very sensitive functions of A_{1g}[34] (see eq 10 and 11). Thus remains the parameter A_{1g}' in Table IV as the only frequency measure for the axial field strength.

As for the parameters ν, r, R, ℓ, and L, which determine the MCD expressions, only the mixing coefficient ν depends on the a_{2u} orbital energy. As may be seen from eq 10 and 13, ν will decrease with increasing one-electron energy of the a_{2u} level. In this respect the spectral study of an axial substitution series is expected to offer a perspective glance along the direction of the ν coordinate for a particular fixed set of the moment integrals. In this simplified picture of the role of axial ligation, the invariance of the moment integrals is a crucial point, which may be verified by using the following sum rules.

$$\bar{\mathcal{D}}_0(G \rightarrow B) + \bar{\mathcal{D}}_0(G \rightarrow Q) = 2e^2(R^2 + r^2)/3$$

$$(\bar{\mathcal{A}}_1/\bar{\mathcal{D}}_0)(G \rightarrow B) + (\bar{\mathcal{A}}_1/\bar{\mathcal{D}}_0)(G \rightarrow Q) = L + \ell \quad (27)$$

From Table IV it is clear that the integral sums $R^2 + r^2$ and $L + \ell$ are seriously affected by ring substituents. As an example the average value of $R^2 + r^2$ is 3.4 Å^2 for the ZnTPP compounds vs. only 2.06 Å^2 for the ZnOEP compounds.[35] Therefore systematic trends may only be studied for a fixed metallo-ring template. Nonetheless even within an axial substitution series of a single metalloporphyrin the moment integrals are not strictly invariant. Although part of this parameter instability is due to experimental uncertainties, some effect of the axial ligators on the moment integrals is undeniable. Especially the dominant terms in eq 27, viz. $\bar{\mathcal{D}}_0(G \rightarrow B)$ and $(\bar{\mathcal{A}}_1/\bar{\mathcal{D}}_0)(G \rightarrow Q)$, show considerable scattering and are of no use to examine the influence of a variation of the coupling coefficient. On the other hand, the weakly allowed terms $\bar{\mathcal{D}}_0(G \rightarrow Q)$, $(\bar{\mathcal{A}}_1/\bar{\mathcal{D}}_0)(G \rightarrow B)$, and also $\bar{\mathcal{B}}_0(G \rightarrow Q)$ are rather insensitive to a limited parameter instability and thus are paramount to monitor the systematic influence of axial ligation. Except for the Soret state angular momentum in the ZnOEP series, these weakly allowed terms indeed turn out to be the ones which vary in a monotonic way with the A_{1g}' frequency measure for the axial field strength.

In the ZnTPP series increasing axial field strength induces a uniform increase of all three weakly allowed Faraday parameters, and the $\bar{\mathcal{B}}_0(G \rightarrow Q)$ term has a normal positive sign. Such a behavior is consistent with Michl's predictions and places the ZnTPP system outside the anomalous [ω,0] region, more specifically on the negative side of this region since a *drop* in ν is accompanied by an *increase* in all three terms. Using eq 25 the total angular variation of ν between ZnTPP in a noncoordinating solvent and ZnTPP(CN) is found to be almost 7°. *Since the ZnTPP series does not extend into the anomalous region, the pivot point ω for the TPP porphyrin cannot be determined from these experiments and even the sign of ω is uncertain.*

In contrast in the ZnOEP series the sign of $\bar{\mathcal{B}}_0(G \rightarrow Q)$ is zero or negative and there is no correlation between the variation of $\bar{\mathcal{D}}_0(G \rightarrow Q)$ and $(\bar{\mathcal{A}}_1/\bar{\mathcal{D}}_0)(G \rightarrow B)$. As we have shown in the previous section both observations are characteristic of the anomalous [ω,0] region on the ν axis. More specifically the almost constant values of the Soret $(\bar{\mathcal{A}}_1/\bar{\mathcal{D}}_0)$ ratio set the ZnOEP series in the parabolic minimum of the $(\bar{\mathcal{A}}_1/\bar{\mathcal{D}}_0)(G \rightarrow B)$ well around the ν origin. As for the exact location of this origin, one may note a slight discrepancy between the variation of A and B terms. Judging from the $(\bar{\mathcal{A}}_1/\bar{\mathcal{D}}_0)(G \rightarrow B)$ values, ZnOEP(py) with the smallest angular momentum should lie closest to $\nu = 0$. However, the point of zero off-diagonal Zeeman mixing is found to coincide with uncoordinated ZnOEP. This difference may be due to systematic errors in the evaluation of the MCD band asymmetries in the Q region. Also, the present model neglects possible zero-field splittings of the degenerate tetragonal states under a low-symmetry axial field. Such splittings are sometimes observable in glassy media at low temperatures.[10,28] It is not unreasonable though to assume that site symmetry lowering effects tend to fade in room-temperature solutions. This seems to be confirmed by the

(33) Antipas, A.; Buchler, J. W.; Gouterman, M.; Smith, P. D. *J. Am. Chem. Soc.* **1980**, *102*, 198.

(34) Wang and Hoffman[6] have indeed experienced that in the ZnTPP series the frequency shifts of $E(B)$ and $E(Q)$ do not yield reliable values for A_{1g}.

(35) Remark that these experimental values are considerably less than the Hückel results of 8.5 Å^2 (see also ref 3, p 99).

fact that there is no apparent relationship between the site symmetry of the axial ligand (C_{2v} for py vs. $C_{\infty v}$ for CN^-) and the global pattern of the MCD spectra.

As the axial field strength increases, the dipole strength of the Q band decreases, as opposed to what was observed in the ZnTPP series. Such a behavior complies with a gradual displacement along the ν axis in the direction of the pivot point ω at a negative angle. The total distance spanned by the present ZnOEP system is calculated to be 6°, which is similar to the $\Delta\nu$ shift in the ZnTPP series. Estimated values of ω range between -14.5° and -12°, depending on whether the ν origin is assigned to the uncoordinated ZnOEP or to ZnOEP(py). Corresponding r/R ratios vary between -0.26 and -0.21. These values are comparable to $r/R = -0.173$, which was obtained by Shelnutt from a spectral fit of OEP metalloporphyrins and related metallouroporphyrins.[8] Inserting reasonable values for the moment integrals in eq 21 yields at $\nu = \omega/2$ a minimal $\bar{\mathcal{B}}_0(G \rightarrow Q)$ value of about -6×10^{-4} $\hbar$ D^2/cm^{-1} (cf. Figure 3). Experimental values turn out to be larger, which again may be due to systematic errors in the extraction of the $\bar{\mathcal{B}}_0$ parameters.

(c) Conclusions. Axial substitution series have been related to small angular distortions around fixed positions in parameter space. The ZnTPP and ZnOEP series have similar $\Delta\nu$ spans but are located in different intervals of the ν axis. Each interval has its own characteristic correlations between the various optical parameters and the average axial field strength. While the ZnOEP data clearly lie in the $[\omega,0]$ interval close to the coordinate origin, the ZnTPP data fall entirely in the normal region at negative ν values. If one assumes similar ω angles for ZnTPP and ZnOEP, ν is found to increase upon replacement of *meso*-phenyl groups by *exo*-alkyl substituents, which is in agreement with the expected influence of ring substituents on the relative positions of the a_{1u} and a_{2u} orbitals[22] (see also section Ib).

As the MCD studies of Djerassi et al. illustrate,[27] complete fluorination[36] of the phenyl substituents in the ZnTPP compounds moves the entire ZnTPP series to the right and into the $[\omega,0]$ interval. The $ZnTF_5PP$ thereby reaches an extreme $\bar{\mathcal{B}}_0(G \rightarrow Q)$ value of -44×10^{-4} $\hbar$ D^2/cm^{-1}, which might very well set this compound in the minimum of the $\bar{\mathcal{B}}_0(G \rightarrow Q)$ well. For $\omega < 0$ axial pyridine or cyanide coordination on $ZnTF_5PP$ is expected to drive the system backwards toward the pivot point ω. Extremely low $\bar{\mathcal{D}}_0(G \rightarrow Q)$ values of only 0.15 D^2 are indeed reported for $ZnTF_5PP(py)$ and $ZnTF_5PP(CN)$, confirming that these complexes enclose the ω point. Quite remarkably in these cases one also observes[27] inverted $\bar{\mathcal{A}}_1(G \rightarrow Q)$ terms. Such sign inversion probably originates from specific vibronic intensity mechanisms, which have not been taken into account in the present model, and only show up around the pivot point where the classical dipole mechanisms tend to cancel.

Finally it should be pointed out that while the different location of different ring templates on the ν axis may indeed be related to the effect of the ring substituents on the HOMO splitting, it must be kept in mind that in principle these substituents may also change the moment integrals and the angle ω, thereby changing the position of the anomalous interval itself.

Further studies on analogous HgTPP and HgOEP compounds are currently in progress.

Acknowledgment. One of us (A.C.) is indebted to the Belgian National Science Foundation (NFWO) for a research grant.

Registry No. ZnTPP, 14074-80-7; ZnTPP(py), 24389-79-5; ZnTPP(CN), 67820-05-7; ZnOEP, 17632-18-7; ZnOEP(py), 54816-40-9; ZnOEP(CN), 99829-69-3.

(36) Spellane, P. J.; Gouterman, M.; Antipas, A.; Kim, S.; Liu, Y. C. *Inorg. Chem.* **1980**, *19*, 386.

Preferred Orientation of Imidazole Ligands in Metalloporphyrins

W. Robert Scheidt* and Daniel M. Chipman*

Contribution from the Department of Chemistry and Radiation Laboratory, University of of Notre Dame, Notre Dame, Indiana 46556. *Received December 26, 1984*

Abstract: Recent work has suggested that axial ligand orientation can affect the physicochemical properties of metalloporphyrins. Analysis of crystallographic data indicates that axial imidazole ligands in metalloporphyrins tend to prefer sterically unfavorable orientations that eclipse equatorial $M-N_p$ bonds. Charge iterative extended Hückel theory calculations on electronic effects for a broad selection of representative systems indicate a previously unrecognized orientational preference in the M-N(imidazole) π bond which favors eclipsed orientations. Somewhat surprisingly, this π bond is found to be dominated by the metal $p\pi$–imidazole $p\pi$ interaction. These theoretical results provide an explanation of the mystery of why the orientation effect seems to be insensitive to metal d^n configuration, spin state, oxidation state, and the presence or absence of a sixth axial ligand.

A number of mechanisms by which physicochemical properties of metalloporphyrins and hemoproteins might be "fine tuned" have been suggested. One of these concerns the orientation of the axial ligands. Geiger et al. have recently suggested[1] that magnetic properties in iron(III) derivatives can depend on the rotational orientation of the axial ligand(s) with respect to the equatorial $M-N_p$ bonds of the porphyrin. This suggestion was based on the correlation of structure with spin state for two crystalline forms of $[Fe(OEP)((3\text{-}Cl)py)_2]^{+}$[2,3] (with radically different electronic states) and the solid-state structure of high-spin $[Fe(OEP)(2\text{-}MeHIm)_2]^{+}$.[1] Korszun et al.[4] have suggested that imidazole

(1) Geiger, D. K.; Lee, Y. J.; Scheidt, W. R. *J. Am. Chem. Soc.* **1984**, *106*, 6336-6343.

(2) (a) Scheidt, W. R.; Geiger, D. K.; Haller, K. J. *J. Am. Chem. Soc.* **1982**, *104*, 495-499. (b) Scheidt, W. R.; Geiger, D. K.; Hayes, R. G.; Lang, G. *J. Am. Chem. Soc.* **1983**, *105*, 2625-2632.

(3) Abbreviations used: Porph, dianion of a generalized porphyrin; P, dianion of porphine; TPP, dianion of *meso*-tetraphenylporphyrin; OEP, dianion of octaethylporphyrin; Proto IX, dianion of protoporphyrin IX; TPivP, dianion of "picket fence" porphyrin; TPyP, dianion of tetra(4-*N*-methylpyridyl)porphine; TPP(Im), dianion of imidazole "tailed" *meso*-tetraphenylporphyrin; Im, generalized imidazole; HIm, imidazole; Im^-, imidazolate anion; 1-MeIm, 1-methylimidazole; 2-MeHIm, 2-methylimidazole; 1,2-Me_2Im, 1,2-dimethylimidazole; BzIm, benzimidazole; 4-$MeHIm^-$, 4-methylimidazolate; (3-Cl)py, 3-chloropyridine; THT, tetrahydrothiophene.

0002-7863/86/1508-1163$01.50/0